Journal of Materials Chemistry A

ROYAL SOCIETY OF CHEMISTRY

PAPER

View Article Online
View Journal | View Issue

Cite this: *J. Mater. Chem. A*, 2024, **12**, 28874

Cross-linking organic cathodes enhances stability at the expense of ionic accessibility†

Ani N. Davis, ‡[a] Kausturi Parui, ‡[b] A M Mahmudul Hasan, [a] Lianett A. Pineda, [b] John D. Langhout, [b] Kiana A. Treaster, [a] Megan M. Butala *[b] and Austin M. Evans *[ab]

Received 24th May 2024
Accepted 20th September 2024

DOI: 10.1039/d4ta03617d

rsc.li/materials-a

We have investigated the fundamental impacts of network cross-linking density on organic cathode performance. Current battery technologies rely on transition metal oxide cathodes that suffer from significant availability, cost, environmental, and humanitarian drawbacks. This reality has inspired the exploration of organic cathode materials that host high theoretical capacities, are environmentally friendly, and are tunable by molecular design. These desirable features are typically accompanied by undesirable instability during battery cycling due to solubility in electrolyte, leading to diminished capacities. Cross-linking polymer electrodes presents one strategy to address dissolution challenges. Here, we synthesized variably cross-linked naphthalene diimide (NDI)-based networks to systematically study the effect of cross-linking density on organic electrode battery performance. NDI-networks were cast as composite electrodes, manufactured into coin cells with lithium metal anodes, and evaluated by galvanostatic cycling. We observed that increased cross-linking facilitated reversible redox-access to NDI units in the network, which correlated to increased stability and capacities. Cathodes with optimized cross-linking host an initial capacity of 106 mA h g^{-1} and >75% capacity retention after 100 cycles with a C/10 rate. This contrasts with uncross-linked materials, which rapidly diminished in performance due to dissolution in the electrolyte, and more densely cross-linked materials, which suffered from limited ionic accessibility. These findings demonstrate that (1) cross-linking can improve organic electrode performance and (2) there are tradeoffs between cycling stability, capacity, and overall energy storage performance with cross-linking density. Future investigations will explore how network design and processing conditions can be leveraged to co-optimize organic cathode performance across these important metrics.

Austin M. Evans

Austin Evans was born and raised in Oklahoma. Austin completed his PhD in Chemistry (2022) at Northwestern University as an NSF Graduate Research Fellow. Austin was a postdoctoral Schmidt Science Fellow at Columbia University working with Professors Latha Venkataraman and Colin Nuckolls. Austin is currently an assistant professor at the University of Florida, where he is a member of the Butler Polymer Laboratory. His research focuses on the precise structural control of macromolecular materials. In his free time, Austin enjoys competing in triathlons.

Introduction

Lithium-ion batteries' high energy density and long-term cycling stability have made them essential to modern life. The need for electrochemical energy storage will grow as electric vehicles, portable electronics, and grid-level energy banks become globally ubiquitous. Currently, commercial lithium-ion batteries rely on graphite anodes and transition metal oxide cathodes.[1] These inorganic cathodes combine modest gravimetric capacities (*e.g.*, 150 mA h g^{-1} for $LiCoO_2$) and high working voltages (4.2 V *vs.* Li^+/Li) with high cycling stabilities.[2,3] While commercial lithium-ion batteries have excellent energy densities, the active materials used in these cathodes rely on expensive elements (*i.e.*, Co, Ni) that have limited availability and rely on harmful mining practices.[4,5] Alternative electrodes that overcome these shortcomings are necessary for next-generation lithium-ion batteries.

[a]*George and Josephine Butler Polymer Laboratory, Department of Chemistry, University of Florida, Gainesville, FL 32611, USA*

[b]*Department of Materials Science and Engineering, University of Florida, Gainesville, FL 32611, USA. E-mail: mbutala@ufl.edu; austinevans@ufl.edu*

† Electronic supplementary information (ESI) available. See DOI: https://doi.org/10.1039/d4ta03617d

‡ Authors contributed equally to this work.

Organic molecules with redox-active motifs are promising candidates for high-performing cathodes.[6] The synthetic versatility of redox-active organic materials can be leveraged to access high theoretical capacities, substantial power densities, and facile processability.[6–8] Anthraquinone, a carbonyl-based small molecule cathode material, has a theoretical capacity of >250 mA h g^{-1} and an energy density of 550 W h kg^{-1}.[9,10] These performance metrics meet the United States Department of Energy's objective to construct Co- and Ni-free batteries with energy densities ≥500 W h kg^{-1} by 2030.[11] While it is challenging to succinctly characterize the state-of-the-art in organic electrode materials, it is apparent that they have significant promise to meet and exceed the performance of inorganic cathodes.[12] However, fundamental structure–property design rules for organic cathodes have yet to be developed.

In particular, the structural and chemical features that lead to high cycling stability in organic electrodes are not well-understood. For example, it is known that anthraquinone suffers from a >50% capacity loss after 20 cycles at a C/10 cycling rate due to dissolution in typical electrolytes (*e.g.* 1 M LiTFSI/1,3-dioxolane + dimethoxyethane (DOL/DME)).[10] This limited stability has motivated research into polymeric electrodes, which are less prone to dissolution than small-molecules. The realization that preventing dissolution improves organic electrode performance has inspired researchers to explore additional approaches to reduce solubility, including increasing polymeric molecular masses,[8] optimizing supramolecular interactions,[12–15] or confining active materials in an insoluble substrate.[16–20] However, a universal method to prevent dissolution while maintaining organic electrode performance has not yet been established.

Another method to reduce the solubility of organic species is to cross-link them into polymer networks, which are inherently insoluble. For example, Lee and coworkers showed rylene-based organic networks constructed by free-radical polymerization could retain >85% of their capacity over 200 cycles at a 1C cycling rate.[21] However, the addition of redox-inactive mass in polymeric systems reduces their energy density, which in this case resulted in the stable rylene networks having a modest gravimetric capacity of <125 mA h g^{-1}. However, cross-linking introduces another challenge, as ionic mobility in densely cross-linked systems may be restricted, which would constrain both the redox-accessibility and power density of these electrodes. Further, the additional mass needed to facilitate cross-linking is also often redox-inactive, which would decrease theoretical capacities. While redox-active polymer networks have been explored previously, dedicated studies to identify the effect of cross-linking density on cathode performance have not yet been performed.

In this report, we systematically assess the effects of cross-linking on electrode performance with a series of naphthalene diimide (NDI)-based polymer networks. By cycling coin cells with NDI-based network active materials with varied amounts of cross-linking in composite cathodes, we uncover the role of cross-linking and molecular interactions on cycling behavior. Generally, we find that cross-linking suppresses electrode dissolution, which improves capacity retention with cycling. However, there is a trade-off between capacity and stability, as there often is for battery electrode materials. We find that the densely cross-linked networks we explore have suppressed ionic conductivity and low capacities, while minorly cross-linked networks have fair initial capacities but poor cycling stability. Intermediately cross-linked networks balance stability and ionic conductivity, demonstrating improved capacity and stability relative to less and more cross-linked networks. We expect that understanding cross-linking effects in polymeric cathodes will provide routes to generate high-performing organic electrodes through intentional synthetic design.

Synthesis and network characterization

To evaluate the impact of cross-linking on electrode performance, we synthesized networks of variable cross-linking density by reacting 1,4,5,8-naphthalenetetracarboxylic dianhydride (NTCDA) with variable ratios of 4,7,10-trioxa-1,13-tridecanediamine (TROX) and tris(2-aminoethyl)amine (TREN) (Fig. 1). We refer to these materials as NDI-*X*, where *X* is the relative molar percent of amines that were derived from the TREN cross-linker. In this naming scheme, NDI-0 is an linear polymer constructed only from TROX diamine (0 mol% TREN), NDI-100 is a fully cross-linked network comprising only TREN triamine (100 mol% TREN), and NDI-50 is a mixture of TROX and TREN with equal molar percent of the amines in the network (50 mol% TREN).

We selected these two amines as our network forming units because of their similar molecular masses per amine, which leads to similar theoretical capacities across the series (118.48 mA h g^{-1} for NDI-0 and 162.62 mA h g^{-1} for NDI-100). In previous studies of NDI networks, styrenic cross-links were used to render NDI insoluble.[21] However, this reduces the materials' hydrophobicity, which decreases ion permeation. We hypothesized that the oligoethylene glycol containing-TROX would provide interactions between Li^+ and our material, providing high ionic accessibilities that are a prerequisite for systematic comparisons between electrode materials.[22]

Imide-linked networks were successfully synthesized by a solvothermal approach. NTCDA was dissolved in DMF under N_2. Combinations of TREN and TROX were then added to the solution simultaneously. The reaction was stirred at 130 °C for 4 hours (see ESI† for additional details). In all reactions, the stoichiometric ratio of amine and anhydride were kept equivalent by considering that TROX and TREN hosted two and three amines, respectively (eqn (S1) through (S3)†). The reaction products rapidly became insoluble upon addition of amine. Following synthesis, these materials were isolated by vacuum filtration, washed with water, acetone, and methanol, and then dried. Following thermal activation, networks with increased incorporation of TROX were darker than those with more TREN (Fig. S15†). Dried NDI-*X* networks were then used for characterization and composite electrode fabrication.

Spectroscopic and thermal characterization indicated the formation of variably cross-linked NDI networks. After polymerization, Fourier-transform infrared spectroscopy (FTIR) showed a disappearance of characteristic anhydride stretches

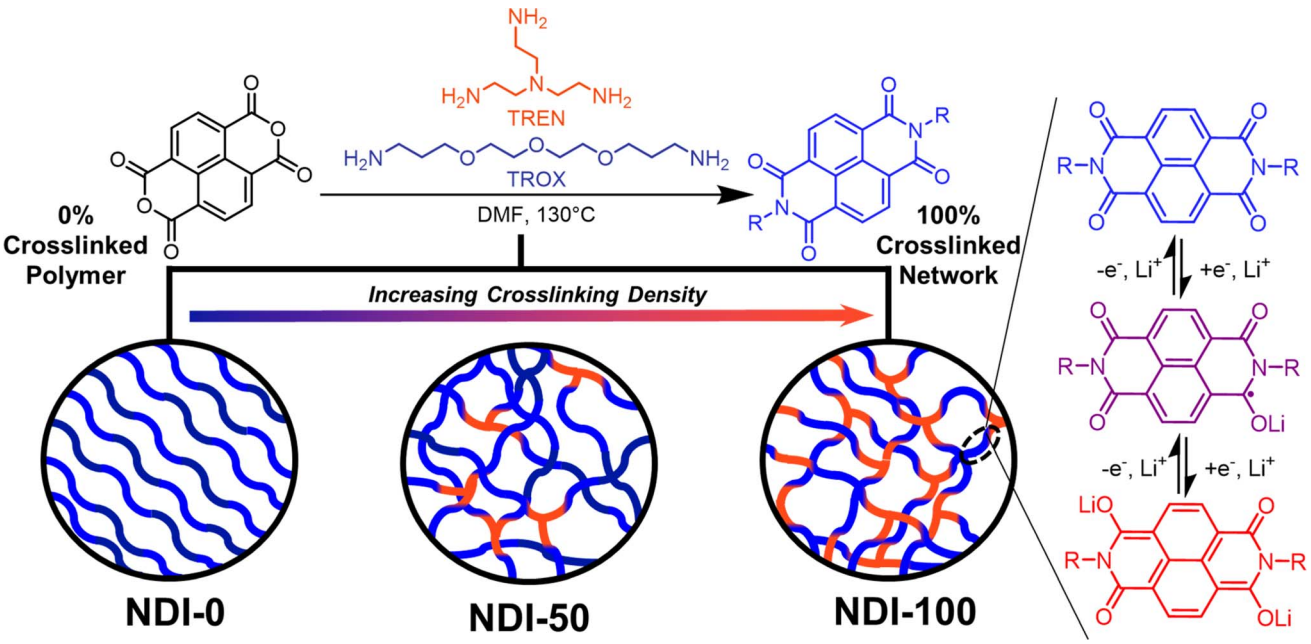

Fig. 1 Synthesis of NDI-*X* and the redox-processes occurring in NDI-*X* cathodes in lithium-ion batteries.

(1750 cm^{-1}) and the appearance of imide features (1700 cm^{-1}, 1662 cm^{-1}) consistent with previous reports (Fig. 2A and S8†).[23–26] To further validate these infrared spectroscopy observations, we synthesized a model compound, *N*,*N*′-dihexyl-1,4,5,8-naphthalenediimide (NDI-hexyl, Fig. S2†). We confirmed the structure of NDI-hexyl using ^{1}H and ^{13}C nuclear magnetic resonance spectroscopy (Fig. S3 and S4†). The infrared spectra of this model compound matched those obtained from insoluble NDI networks. Infrared spectroscopy of the NDI-*X* networks also showed subtle differences in the relative intensities of features at 1105 cm^{-1} and 875 cm^{-1}, which we assign to the differential incorporation of TREN and TROX (Fig. 2A).

Consistent with these infrared spectroscopy observations, thermogravimetric analysis also confirmed that higher cross-linking ratios were obtained when more TREN was used. At higher cross-linking densities, we found the residual mass at 600 °C increased consistently from 27% to 60% from NDI-0 to NDI-100 (Fig. 2B). The T_{95} of these networks decreased from 400 °C to 323 °C with an increased incorporation of TREN. Non-conjugated C–N single bonds have lower bond energies resulting in more cross-linked materials being more thermally labile and leading to higher char yields.[27] Together, these observations confirm that the conversion during network formation with variable amounts of TREN and TROX is near-quantitative.

Microstructural characterization of the NDI-*X* active materials revealed that these materials are prepared as amorphous particles. X-ray diffraction performed on the NDI-*X* networks revealed that cross-linking densities >50% (NDI-50, 75, 100) were entirely amorphous. Lower cross-linking densities

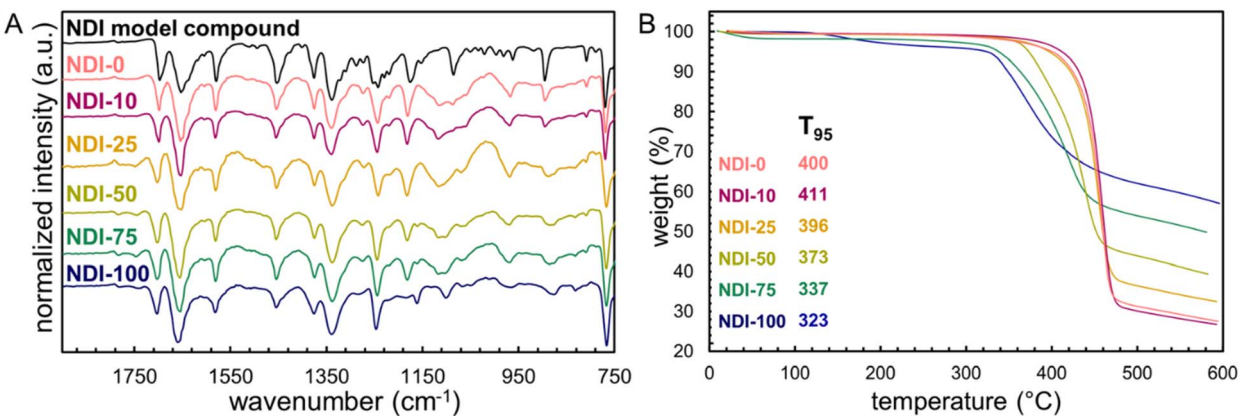

Fig. 2 Chemical and thermal characterization of NDI-*X* cathodes. (A) FTIR spectra of NDI-hexyl model compound and NDI networks with increasing cross-linking density. (B) TGA profile of NDI networks with T_{95} values displayed for clarity.

resulted in weakly diffracting materials that have features consistent with the π–π stacking (20°–30°) of the aromatic NDI cores used in this study (Fig. S17†). Scanning electron microscopy reveals an evolution in particle morphology as a function of cross-linking (Fig. S18†). We observe that NDI-0 and NDI-10 have a flaky texture which contrasts the spheroidal particles of the highly cross-linked networks (NDI-50, 75, 100). NDI-25 had multiple phases with both wavy and flaky particles being present in the same sample. These observations are consistent with the poorly defined nanostructure we assign from these networks' X-ray diffraction patterns.

Battery cycling and electrochemical behavior

Coin cells assembled with cast composite NDI-*X* cathodes (active material : conductive carbon additive : polyvinylidene fluoride binder in 6 : 3 : 1 ratio by mass) and Li metal anodes were cycled galvanostatically between 1.5 V and 3.5 V. Galvanostatic cycling with potential limitations (GCPL) experiments were used to compare cycling profiles, capacities, and rate capabilities of NDI-based networks, which provided mechanistic insights into the effects of cross-linking on organic cathode performance. We find that cross-linking modified the nature of electrochemical profiles, the formation behavior of the cells, and the achievable capacity following formation cycles.

Cycling behavior was influenced by network cross-link density. This is apparent in the GCPL profiles of the sixth cycle for all of the NDI-*X* electrodes cycled at C/10 (Fig. 3A and S10B†). The profiles of less cross-linked electrodes (NDI-0, NDI-10, NDI-25) had two well-defined electrochemical processes (Fig. 3A), consistent with the separate redox processes identified in cyclic voltammetry of an NDI model compound, NDI-hexyl (Fig. S9†). However, these two electrochemical processes become less resolved at higher cross-linking densities (NDI-50, NDI-75, NDI-100). We attribute this evolution to changes in the kinetic limitations associated with ion transport in cathode electrodes.

The relative definition of the two electrochemical processes occurring during cycling in the NDI-*X* electrodes is more pronounced when viewed as the differential capacity with respect to voltage (Fig. 3B and S10D†). For all of the prepared networks, regardless of cross-link density, some fraction of NDI redox-centers were doubly reduced and were electronically and ionically accessible (Fig. 1). Differential capacity plots of intermediate cross-linking densities (NDI-25 and NDI-75) showed two symmetric redox-events that were separated by 250 mV (at 2.55 V and 2.25 V *vs.* Li^+/Li, respectively). In less cross-linked electrodes we observed features that were further separated (for NDI-0, 2.3 V and 2.6 V *vs.* Li^+/Li) (Fig. 3B). For the differential capacity plot of NDI-100 we observed the opposite with redox features being closer together and less defined (Fig. 3B). With higher cross-linking density, the two processes became less distinct. Specifically, for NDI-100, the overpotential increased, indicating additional energy required for lithiation and delithiation (Fig. 3A). The increased hysteresis between the symmetric processes during discharge and charge for NDI-100 reflected that the overpotential was due to kinetic – rather than energetic – differences, most likely due to ionic transport limitations associated with high cross-linking density.

Cross-linking density impacted the formation behavior and the degree of overcharge in NDI-*X* cathodes (Fig. 3C). NDI-0 showed consistent overcharging during cycling, indicating that the charge capacity exceeded the prior discharge capacity. This indicates that redox reactions occur in solution as a result of species – likely NDI-based oligomers – dissolving in the electrolyte, resulting in a loss of active material during cycling. This process is reminiscent of the well-documented dissolution of polysulfide species in Li–S batteries and subsequent overcharging *via* the "polysulfide shuttle".[28] Overcharging and associated degradation contributed to the rapid decrease of capacity during the first 5 cycles and the low overall performance of NDI-0 (Fig. 3C).

Cross-linked NDI networks had formation cycles (or induction periods) and less overcharging than NDI-0, suggesting that dissolution is suppressed with cross-linking and that cross-linked NDI networks underwent structural equilibration during initial cycles (Fig. 3A and C). Such an induction period is commonly observed in other classes of electrodes, such as in cross-linked sulfide electrodes used in lithium–sulfur batteries.[29] The continual increase in capacity reflected that, with each cycle, more redox-active material can participate in energy storage. We attribute this increased capacity to enhanced intermolecular interactions in NDI-*X* cathodes between redox-active NDI subunits, the conductive additive, and lithium ions. We expect that the ion-intercalation mechanism is a combination of ion hopping and local segmental chain motion, similar to mechanisms of lithium-ion transport previously reported for amorphous cross-linked organic electrolytes.[30] For partially cross-linked NDI networks, capacity increased during initial cycles, stabilizing in the first 6 cycles (Fig. 3C, 4A and 4C). However, fully cross-linked NDI-100 had a low initial capacity that increased more slowly than partially cross-linked networks, not stabilizing within the first 20 cycles (Fig. 3C). We propose that the rigidity and closer molecular packing of the NDIs prevented efficient ion accessibility in NDI-100. After the induction period of most compositions, NDI networks achieved moderate fractions of their theoretical capacities in cycle 6 (59%, 48%, 43%, 78%, 70%, and 14% for NDI-0, NDI-10, NDI-25, NDI-50, NDI-75, and NDI-100, respectively; Fig. 3A and S8B†).

NDI networks have a reduced charge-transfer resistance after undergoing formation cycles. To further investigate the improvement in capacity, we performed electrochemical impedance spectroscopy (EIS) before and after the formation cycles. We observed a significant decrease in charge-transfer resistance (R_{ct},) between the electrode materials and electrolyte for all networks with a cross-linking density less than NDI-100 (between 68% and 84% reduction for NDI-0 through NDI-75, Fig. S6 and S7†). We attribute the decrease in R_{ct} to microstructural changes that create more-defined charge transport pathways yielding higher observed capacities. This could be

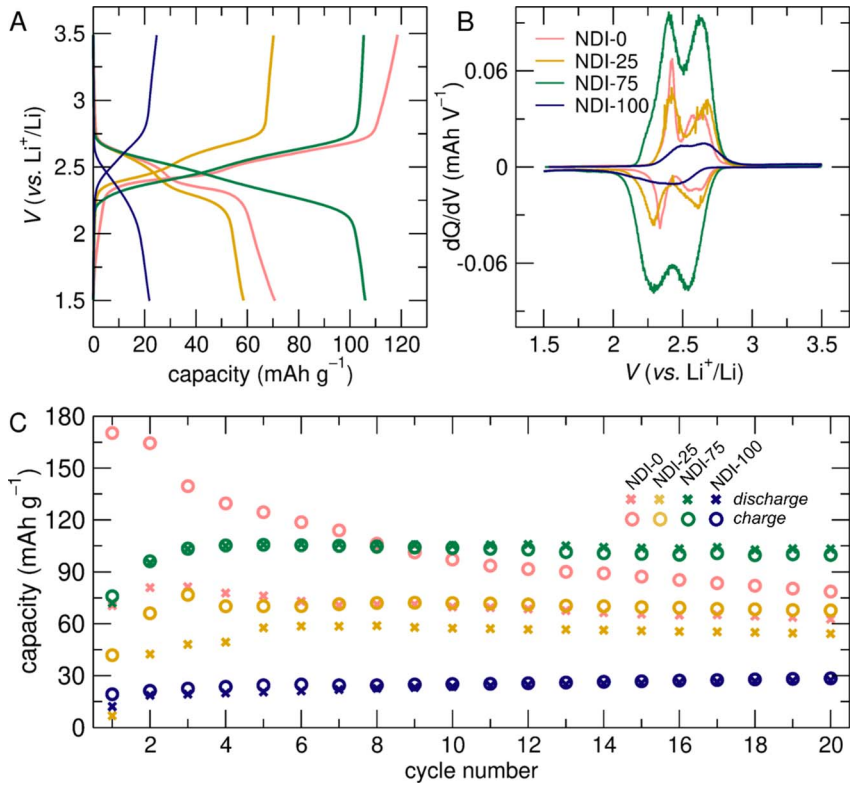

Fig. 3 Electrochemical characterization for NDI-*X* electrodes. (A) GCPL charge–discharge curves for cycle 6 at C/10. (B) Differential capacity plots for the GCPL shown in panel A. (C) Charge and discharge capacity for NDI-*X* cells during the first 20 cycles.

attributed to an increased in enthalpically preferred π–π stacking of NDI units. Comparatively, NDI-100 saw a minimal decrease in R_{ct} than the other cross-linked electrodes (6.3% decrease) (Fig. S7D†). This is consistent with the hypothesis that NDI-100 is too rigid to undergo structural changes to allow for the facile establishment of charge-transfer pathways. Future

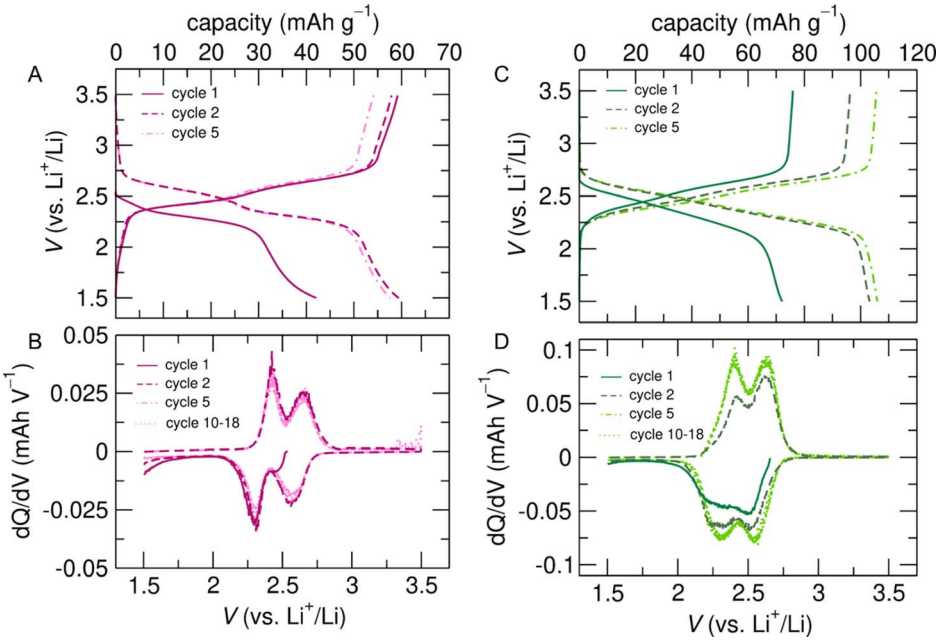

Fig. 4 Comparative cathode performance between NDI-10 and NDI-75. GCPL for (A) NDI-10 and (C) NDI-75 collected at C/10 rate. Differential capacity plots for (B) NDI-10 and (D) NDI-75.

investigations into organic electrodes would benefit from a deeper understanding of the evolving microstructure of amorphous polymeric materials upon electrochemical cycling.

In addition to capacity, cycling profiles also evolved during the induction period. This is highlighted for NDI-10 and NDI-75, which both had relatively high overpotentials during the first discharge. The capacity of NDI-10 quickly increased, with this cell achieving its highest capacity during the second cycle (Fig. 4A). NDI-10 also shows overcharging during the first charge. In contrast, the capacity of NDI-75 increased more gradually, achieving a higher maximum capacity than NDI-10. Specifics of formation and maximum capacity varied between cells with the same cross-linking. For NDI-75, cell-to-cell variation included differences in the degree of overcharging. We attribute the increase in discharge capacity and decrease in overpotential after the first cycle in Fig. 4A and B to changes in local morphology within cross-linked network cathodes. As the cell is cycled, previously inaccessible electrode material is revealed through microstructure evolutions in the electrode active material. These architecture changes allow ions to intercalate into the material more homogenously and drive the establishment of more regular ion-conduction pathways. While the data in Fig. 4B did not show overcharging, other cells did (Fig. S16†). This suggests that the structural evolution occurring during the induction period are occurring over length scales larger than the local NDI-units.

Differential capacity plots show that the electrochemical features of NDI-10 stabilized within the first cycle with two distinct features that are reproduced in later cycles (Fig. 4B). For NDI-75, there was an evolution of electrochemical features, stabilizing at cycle 5 with two symmetrical features (Fig. 4D). The higher capacities, shifts in redox potentials, and increased cycling stability seen for NDI-75 indicates that intermediate cross-link densities allow for optimized π–π stacking between NDI redox units. This implies that cross-linking density and supramolecular interactions may provide an approach to tune redox potentials and electrochemical accessibility in organic cathodes.[31]

Moderate degrees of cross-linking in NDI promoted cycling stability by mitigating dissolution while maintaining redox-accessibility. The cycling stability of the material was evaluated by cycling at a C/10 rate for more than 80 days (100 cycles). The relatively slow cycling rate ensures that kinetically limited degradation processes are obvious and are representative of rechargeable energy storage applications. NDI-75 had the highest overall capacity and retained >90% of the 6th cycle capacity after 50 cycles and >75% after 100 cycles at a C/10 cycling rate highlighting a balance of accessibility and stability within the moderately cross-linked network (Fig. 5). The gradual decline in capacity appeared to result from slight irreversibility between discharge and charge processes in these cathodes. By comparison, less cross-linked NDI-10 consistently exhibited higher capacities on charge than discharge and had a capacity retention of only 60% from cycle 6 to 100 at C/10, suggesting strongly operative dissolution. In contrast, more cross-linked NDI-100 had a >50% increase in capacity over 100 cycles, reaching <40 mA h g^{-1}. We attribute this capacity change

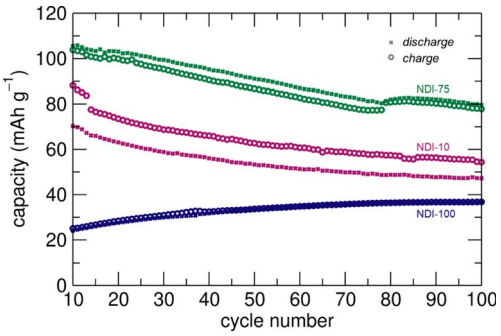

Fig. 5 Long-term cycling stability of NDI-10, NDI-75, NDI-100 for cycles 10–100. Cells were cycled at a C/10 rate.

to a slow induction period, during which previously inactive NDI-subunits become accessible as the microstructure evolves with cycling.[29,32] While these data suggest that NDI-100 has high cycling stability, it also demonstrates that the inherent inflexibility of densely cross-linked NDI-100 leads to poor ionic conductivity and as a result, poor rate performance.

The optimally cross-linked NDI-75 cathode showed a good balance between ionic conductivity and stability, which was quantified by GCPL at variable cycling rates between C/10 and 8C. Variable rate cycling for NDI-75 showed a decrease in degree of overcharge (Fig. S13†) and an increase in overpotential (Fig. 6) with increasing cycling rate. Similar trends were seen in other intermediately cross-linked NDI networks (*e.g.*, NDI-25, Fig. S14†). With increasing cycling rate, the achievable capacity decreased. For NDI-75 the capacity decreased from 105 mA h g^{-1} to 60 mA h g^{-1} between C/10 and 8C (Fig. 6). This decrease corresponded to a 42% capacity retention with an 80× increase in cycling rate. Cycling curves were also symmetric at all rates, which suggests that electrochemical reversibility was maintained over this cycling rate range (Fig. 6) and is consistent with the full recovery of capacity at C/10 after exposing the

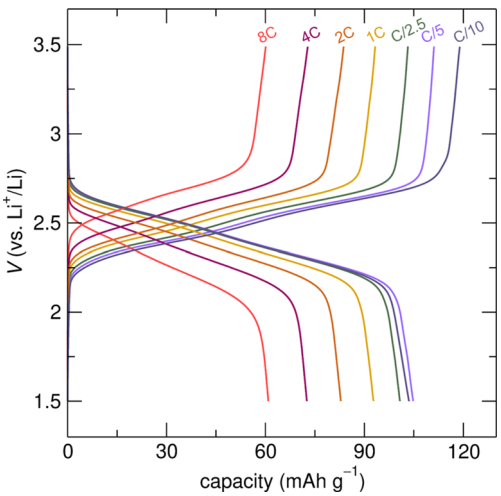

Fig. 6 Galvanostatistically cycled NDI-75 at variable rates from C/10 to 8C. The first cycle at each rate is shown here. The first C/10 has been omitted as NDI-75 undergoes induction for the first 6 cycles.

electrodes to higher cycling rates (Fig. S13†). These variable rate cycling experiments performed on NDI-75 show that while dissolution and ionic accessibility must be co-optimized, they are not mutually orthogonal.

Processing cross-linked organic cathodes

In conducting this work, we found cycling behavior was significantly impacted by electrode preparation. Several different approaches to electrode processing yielded quite different results, which we share here in hopes of benefiting future work in insoluble organic electrodes. Ultimately, we conceived of an approach to process NDI networks into slurries with conductive carbon additive, binder, and a binder solvent that were cast into smooth films on Al foil. Cycling data using these electrodes showed cell-to-cell variability within expectations of organic electrode materials (Fig. S16†). Further, we found that intermediately cross-linked networks were more reproducible than uncross-linked and fully cross-linked networks (NDI-0 and NDI-100, respectively).

Initially, we screened the cycling behavior of NDI networks using loose-powder composite electrodes in Swagelok half-cells. For these, active material was combined with conductive carbon and PTFE binder (6 : 3 : 1 ratio by mass) in an agate mortar and pestle. GCPL of these cells showed two reversible redox processes (Fig. S5†), consistent with the model NDI compound and coin cells with cast electrodes. However, the achievable capacities with loose-powder electrodes were significantly lower. NDI-50, for example, had a maximum capacity over 100 mA h g^{-1} in coin cells, but less than 20 mA h g^{-1} in the loose-powder Swagelok cells (Fig. S5†). This low capacity inspired us to explore if electrolyte wettability may pose a difficulty in a Swagelok configuration. However, contact angle experiments demonstrated that electrolyte wettability was not significantly impacted by cross-linking (Fig. S19†). Therefore, these low capacities are likely due to challenges with contact in the loose-powder electrodes, either between the active material and conductive carbon additive or between the powder and current collector.

To more appropriately assess the overall and relative behavior of NDI networks, we adapted processes typically used in the preparation of cast electrodes with inorganic active materials from a slurry. Inorganic electrodes slurries are typically prepared by combining the active material with conductive carbon, binder, and a solvent for the binder through shear mixing – either by hand or using a centrifugal mixer. These processes did not yield smooth casts (Fig. S5†), indicating inhomogeneous distributions of electrode constituents. However, we found that smooth casts could be prepared from a more homogeneous suspension of constituent electrode components, achieved by stirring them in the binder solvent, *N*-methylpyrolidone, for two days. By this method, more homogeneous and consistent electrodes could be cast onto aluminum foil by doctor blading (Fig. S5†). Cycling these electrodes in coin cells resulted in improved capacities and lower cell-to-cell variability, allowing fundamental chemical insights of the effects of cross-link density in NDI networks to be derived. We hope these findings will accelerate future efforts toward systematically processing and assessing insoluble and cross-linked organic electrode materials.

Conclusions

We demonstrate that cross-linking is an effective strategy to suppress dissolution of organic cathodes. Galvanostatic cycling experiments showed that intermediate cross-linking densities (NDI-25–NDI-75) have the most symmetric charge–discharge behavior, highest capacity retention, and most effective cycling stability of the electrode compositions we investigated. Intermediate cross-linking densities in NDI-75 lead to optimized energy densities (252.7 W h kg^{-1}) and cycling performances (75% over 100 cycles C/10). This desirable stability was accompanied by moderate rate performance with a capacity drop of 57% between C/10 to 8C. Less cross-linked NDI-networks (NDI-0 and NDI-10) are prone to dissolution, which leads to lower cycling stabilities. However, more densely cross-linked materials have ion accessibility challenges that lead to lower overall capacities and higher numbers of formation cycles. This report demonstrates that cross-linking can be used to enhance the dissolution resistance of organic electrodes without precluding redox-accessibility. This work suggests that co-developing network design and processing is a potential route to developing highly stable and high-performing organic cathode materials.

Data availability

The data supporting this article have been included as part of the ESI† and the data that support the findings of this study are available from the corresponding authors upon reasonable request.

Author contributions

A. N. D. conceived the experiments, synthesized the polymer networks, and characterized their electrode performance. K. P. assembled cells, designed and executed battery performance experiments, and analyzed battery data. L. A. P. assisted in electrode synthesis and characterization. M. H. assisted with electrochemical characterization. K. A. T. assisted with material characterization (XRD). J. D. L. assisted with material characterization (SEM). A. N. D. and K. P. wrote the initial drafts of the manuscripts. M. M. B. and A. M. E. contributed to experimental design and supervised this work. All authors contributed to the writing of this manuscript.

Conflicts of interest

The authors declare they have no conflict of interest.

Acknowledgements

This work was partly conducted at the Nanoscale research Facility of the Herbert Wertheim College of Engineering at the University of Florida. K. A. T. was supported by the Department of Defense (DoD) through the National Defense Science & Engineering Graduate (NDSEG) Fellowship Program. We thank the Department of Defense for a Multidisciplinary University Research Initiative Award (W911NF2310260) that supported K. A. T.'s thesis work.

Notes and references

1 J. Xie and Y.-C. Lu, *Nat. Commun.*, 2020, **11**, 2499.
2 A. Manthiram, *Nat. Commun.*, 2020, **11**, 1550.
3 M. Armand and J. M. Tarascon, *Nature*, 2008, **451**, 652–657.
4 C. L. N. Banza, T. S. Nawrot, V. Haufroid, S. Decrée, T. De Putter, E. Smolders, B. I. Kabyla, O. N. Luboya, A. N. Ilunga, A. M. Mutombo and B. Nemery, *Environ. Res.*, 2009, **109**, 745–752.
5 C. Banza Lubaba Nkulu, L. Casas, V. Haufroid, T. De Putter, N. D. Saenen, T. Kayembe-Kitenge, P. Musa Obadia, D. Kyanika Wa Mukoma, J.-M. Lunda Ilunga, T. S. Nawrot, O. Luboya Numbi, E. Smolders and B. Nemery, *Nat Sustainability*, 2018, **1**, 495–504.
6 Y. Lu and J. Chen, *Nat. Rev. Chem*, 2020, **4**, 127–142.
7 Y. Liang and Y. Yao, *Joule*, 2018, **2**, 1690–1706.
8 Z. Wu, Q. Liu, P. Yang, H. Chen, Q. Zhang, S. Li, Y. Tang and S. Zhang, *Electrochem. Energy Rev.*, 2022, **5**, 26.
9 S.-J. Yang, X.-Y. Qin, R. He, W. Shen, M. Li and L.-B. Zhao, *Phys. Chem. Chem. Phys.*, 2017, **19**, 12480–12489.
10 W. Li, L. Chen, Y. Sun, C. Wang, Y. Wang and Y. Xia, *Solid State Ionics*, 2017, **300**, 114–119.
11 National Blueprint for Lithium Batteries, **https://www.energy.gov/sites/default/files/2021-06/FCABNationalBlueprintLithiumBatteries0621_0.pdf**, accessed April 2024.
12 A. N. Davis, K. Parui, M. M. Butala and A. M. Evans, *Nanoscale*, 2024, **16**(21), 10142–10154.
13 T. Chen, H. Banda, L. Yang, J. Li, Y. Zhang, R. Parenti and M. Dincă, *Joule*, 2023, **7**, 986–1002.
14 S. Louie, Y. Zhong, S. T. Bao, C. Schaack, A. Montoya, Z. Jin, N. M. Orchanian, Y. Liu, W. Lei, K. Harrison, J. Hone, A. Angerhofer, A. M. Evans and C. P. Nuckolls, *J. Am. Chem. Soc.*, 2023, **145**, 4940–4945.
15 M. J. Strauss, A. M. Evans, E. K. Roesner, R. J. Monsky, M. I. Bardot and W. R. Dichtel, *Acc. Mater. Res.*, 2022, **3**, 935–947.
16 H. Wu, K. Wang, Y. Meng, K. Lu and Z. Wei, *J. Mater. Chem. A*, 2013, **1**, 6366–6372.
17 A. E. Baumann, X. Han, M. M. Butala and V. S. Thoi, *J. Am. Chem. Soc.*, 2019, **141**, 17891–17899.
18 B. Liu, A. E. Baumann, M. M. Butala and V. S. Thoi, *Chem.–Eur. J.*, 2023, **29**, e202300821.
19 S. Lv, X. Ma, S. Ke, Y. Wang, T. Ma, S. Yuan, Z. Jin and J.-L. Zuo, *J. Am. Chem. Soc.*, 2024, **146**, 9385–9394.
20 K. A. Treaster, A. N. Davis, M. M. Butala and A. M. Evans, *Trends Chem.*, 2024, **6**(9), 503–505.
21 S. U. Sharma, Y.-L. Chang, S. V. Chaganti, Y. W. More and J.-T. Lee, *ACS Appl. Energy Mater.*, 2022, **5**, 7550–7558.
22 M. J. Strauss, I. Hwang, A. M. Evans, A. Natraj, X. Aguilar-Enriquez, I. Castano, E. K. Roesner, J. W. Choi and W. R. Dichtel, *J. Am. Chem. Soc.*, 2021, **143**, 17655–17665.
23 Z. Jin, Q. Cheng, A. M. Evans, J. Gray, R. Zhang, S. T. Bao, F. Wei, L. Venkataraman, Y. Yang and C. Nuckolls, *Chem. Sci.*, 2022, **13**, 3533–3538.
24 A. M. Evans, K. A. Collins, S. Xun, T. G. Allen, S. Jhulki, I. Castano, H. L. Smith, M. J. Strauss, A. K. Oanta, L. Liu, L. Sun, O. G. Reid, G. Sini, D. Puggioni, J. M. Rondinelli, T. Rajh, N. C. Gianneschi, A. Kahn, D. E. Freedman, H. Li, S. Barlow, G. Rumbles, J.-L. Brédas, S. R. Marder and W. R. Dichtel, *Adv. Mater.*, 2022, **34**, 2101932.
25 S. Jhulki, C. H. Feriante, R. Mysyk, A. M. Evans, A. Magasinski, A. S. Raman, K. Turcheniuk, S. Barlow, W. R. Dichtel, G. Yushin and S. R. Marder, *ACS Appl. Energy Mater.*, 2021, **4**, 350–356.
26 Z. Jin, Q. Cheng, S. T. Bao, R. Zhang, A. M. Evans, F. Ng, Y. Xu, M. L. Steigerwald, A. E. McDermott, Y. Yang and C. Nuckolls, *J. Am. Chem. Soc.*, 2022, **144**, 13973–13980.
27 Y. Zhou, Z. Zhang, Q. Tang, X. Ma and X. Hou, *Mater. Horiz.*, 2024, **11**(18), 4348–4358.
28 Y. V. Mikhaylik and J. R. Akridge, *J. Electrochem. Soc.*, 2004, **151**, A1969–A1976.
29 M. B. Preefer, B. Oschmann, C. J. Hawker, R. Seshadri and F. Wudl, *Angew. Chem., Int. Ed.*, 2017, **56**, 15118–15122.
30 J. Lopez, D. G. Maxkanic, Y. Cui and Z. Bao, *Nat. Rev. Mater.*, 2019, **4**, 312–330.
31 N. Kumari, S. Naqvi and R. Kumar, *J. Mater. Sci.*, 2018, **53**, 4046–4055.
32 M. M. Butala, K. R. Danks, M. A. Lumley, S. Zhou, B. C. Melot and R. Seshadri, *ACS Appl. Mater. Interfaces*, 2016, **8**, 6496–6503.